Analysis of the flow behavior of concentrated polymer solutions through transient network models. Part II, general two-dimensional flow

J. Zaragoza and O. Manero

Departamento de Polímeros, Instituto de Investigaciones en Materiales,
Universidad Nacional Autónoma de México, Apdo. Postal 70-360,
04510 México, D.F.

Abstract. The network model with conformation-dependent non-affine motion discussed in Part I, is generalized to cover flows ranging from simple shear to elongational. A flow parameter λ is defined to specify the particular type of two-dimensional flow. The values of zero and one correspond to simple-shear and pure extensional flow respectively. It is shown that non-affine motion is important in flows sufficiently close to simple shear, where the correlation of birefringence with the eigenvalue of the velocity gradient tensor holds, if conformation-dependency is considered. This is in agreement with experimental results performed in two corrotating rollers using 2 concentrated polymer solutions.

Resumen. Los modelos de redes discutidos en la parte I son generalizados para discutir diferentes tipos de flujos, desde el cortante simple hasta el elongacional. Para especificar el tipo de flujo bidimensional se define un parámetro de flujo λ tal que los valores de cero y uno corresponden a flujos cortantes y elongacionales, respectivamente. Se demuestra que el movimiento no afín es importante en flujos suficientemente cercanos al cortante simple, donde prevalece la correlación de la birrefringencia con el valor propio del tensor gradiente de velocidades. Estas predicciones muestran concordancia con resultados experimentales realizados en un sistema de dos rodillos corrotatorios empleando dos soluciones concentradas de polímeros.

1. Introduction

As it was shown in Part I, non-affine motion in network models is an important idea if predictions for the flow of concentrated polymeric systems of flexible macromolecules are sought. In addition, effects due to nonlinear forces in the segments making up the network were also shown. The evolution equation for the distribution function of the segments end-to-end distance was expressed as

$$\frac{\partial \Psi}{\partial t} + \nabla \cdot \dot{\mathbf{r}} \Psi = G - \beta \Psi, \tag{1}$$

where

$$\dot{\mathbf{r}} = \mathbf{L} \cdot \mathbf{r}, \tag{2}$$

$$\mathbf{L} = \mathbf{\Gamma} - \epsilon \mathbf{D}, \tag{3}$$

$$\epsilon = \epsilon(\langle r^2 \rangle) = \frac{\epsilon_0}{N \langle r^2 \rangle + 3} \tag{4}$$

and

$$\beta = \frac{\beta_0}{1 - \langle r^2 \rangle}. \tag{5}$$

In this work, a general two dimensional planar flow is considered. It is generally accepted that flows with elongational components can produce relatively larger deformations on the macromolecules than those produced by simple shear flows. To demonstrate this point, it is important to relate the measure of the deformation of the network, *i.e.*, the birefringence, with both the flow type and the velocity gradient.

2. A general two-dimensional flow

In this case, the velocity-gradient tensor $\mathbf{\Gamma}$ is given by

$$\mathbf{\Gamma} = \frac{\dot{\gamma}}{2} \begin{pmatrix} (1+\lambda) & (1-\lambda) & 0 \\ -(1-\lambda) & -(1+\lambda) & 0 \\ 0 & 0 & 0 \end{pmatrix}, \tag{6}$$

where $\dot{\gamma}$ is the magnitude of the velocity gradient, $\lambda = 1$ defines a planar elongational flow (hyperbolic flow), $\lambda = 0$ represents simple-shear flow and values ranging from zero to one cover mixed-type flows with a proportion of elongational components.

Fig. 1 depicts the planar flows obtained by varying the parameter λ.
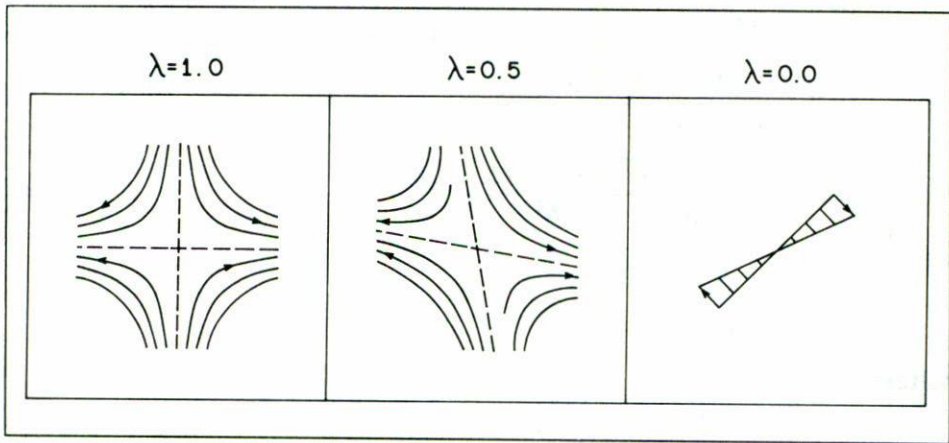

FIGURE 1. Various types of two-dimensional flows. $\lambda = 1$ corresponds to planar elongation and $\lambda = 0$ specifies simple shear flow.

To generalize the equations for the momenta of the distribution function, it is necessary to include the flow parameter λ in Eq. (16) of Part I. By considering (6), these are:

$$\frac{d\langle x^2 \rangle}{dt} + \left[h - \alpha(\lambda + 1)(1 - \epsilon[\langle r^2 \rangle]) \right] \langle x^2 \rangle = -\alpha(1 - \lambda)\langle xy \rangle + \frac{L}{3N\beta_0},$$

$$\frac{d\langle y^2 \rangle}{dt} + \left[h + \alpha(\lambda + 1)(1 - \epsilon[\langle r^2 \rangle]) \right] \langle y^2 \rangle = \alpha(1 - \lambda)\langle xy \rangle + \frac{L}{3N\beta_0},$$

$$\frac{d\langle xy \rangle}{dt} + h\langle xy \rangle = \frac{\alpha}{2}(1 - \lambda)\langle y^2 \rangle - \frac{\alpha}{2}(1 - \lambda)\langle x^2 \rangle \tag{7}$$

and

$$\frac{d\langle z^2 \rangle}{dt} + h\langle z^2 \rangle = \frac{L}{3N\beta_0},$$

where

$$h = \frac{\beta}{\beta_0} = \frac{1}{1 - \langle r^2 \rangle} \qquad \text{and} \qquad \alpha = \frac{\dot{\gamma}}{\beta_0}.$$

In steady-state, Eq. (7) are easily solved. The expressions for the momenta are:

$$\langle x^2 \rangle = \frac{L}{3N\beta_0 h} \left[\frac{h^2 + \alpha h(1 + \lambda)(1 - \epsilon[\langle r^2 \rangle]) + \alpha^2(1 - \lambda)^2}{h^2 - \alpha^2 v} \right],$$

$$\langle y^2 \rangle = \frac{L}{3N\beta_0 h} \left[\frac{h^2 - \alpha h(1 + \lambda)(1 - \epsilon[\langle r^2 \rangle]) + \alpha^2(1 - \lambda)^2}{h^2 - \alpha^2 v} \right],$$

$$\langle xy \rangle = \frac{-L}{3N\beta_0 h} \left[\frac{\alpha^2(1 + \lambda^2)(1 - \epsilon[\langle r^2 \rangle])}{h^2 - \alpha^2 v} \right] \tag{8}$$

and

$$\langle z^2 \rangle = \frac{L}{3N\beta_0 h},$$

where

$$v = (1 + \lambda)^2(1 - \epsilon[\langle r^2 \rangle]) - (1 - \lambda)^2. \tag{9}$$

Birefringence measured in the (x, y) plane is given by

$$\frac{\Delta_n}{B} = \frac{2L}{3N\beta_0 h} \left[\frac{\alpha(1 + \lambda)(1 - \epsilon[\langle r^2 \rangle])}{h(h^2 - \alpha^2 v)} \right] \sqrt{h^2 + \alpha^2(1 - \lambda)^2}. \tag{10}$$

3. Results

Predictions from Eq. (10) are given in Figs. 2–5. In Fig. 2, the birefringence is plotted with the velocity gradient for several values of the flow parameter $\lambda(0.001 \leq \lambda \leq 1)$ considering affine motion ($\epsilon = 0$).

Higher deformations are obtained when the proportion of elongational components is larger for a given value of the velocity gradient. It is observed an almost fully stretched conformation of the segments for $\lambda = 1$, corresponding to elongational flow at relatively small values of the velocity gradient.
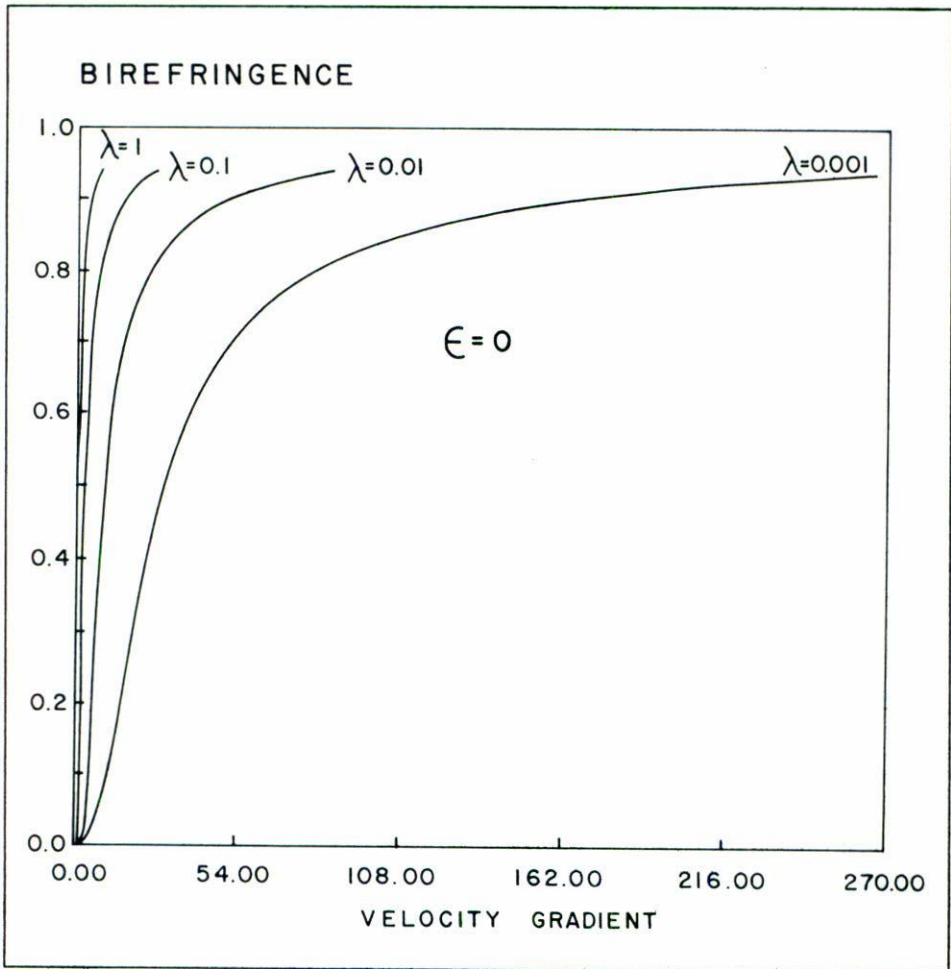
BIREFRINGENCE

FIGURE 2. Normalized flow birefringence vs. velocity gradient for various flow types (λ). Affine motion.

However, when these curves are plotted with the eigenvalue of the velocity gradient tensor $\alpha\sqrt{\lambda}$, correlation is obtained. This is shown in Fig. 3 demonstrating that the birefringence (or any invariant of the tensor **rr**) scales with $\alpha\sqrt{\lambda}$ for a wide range of λ. This
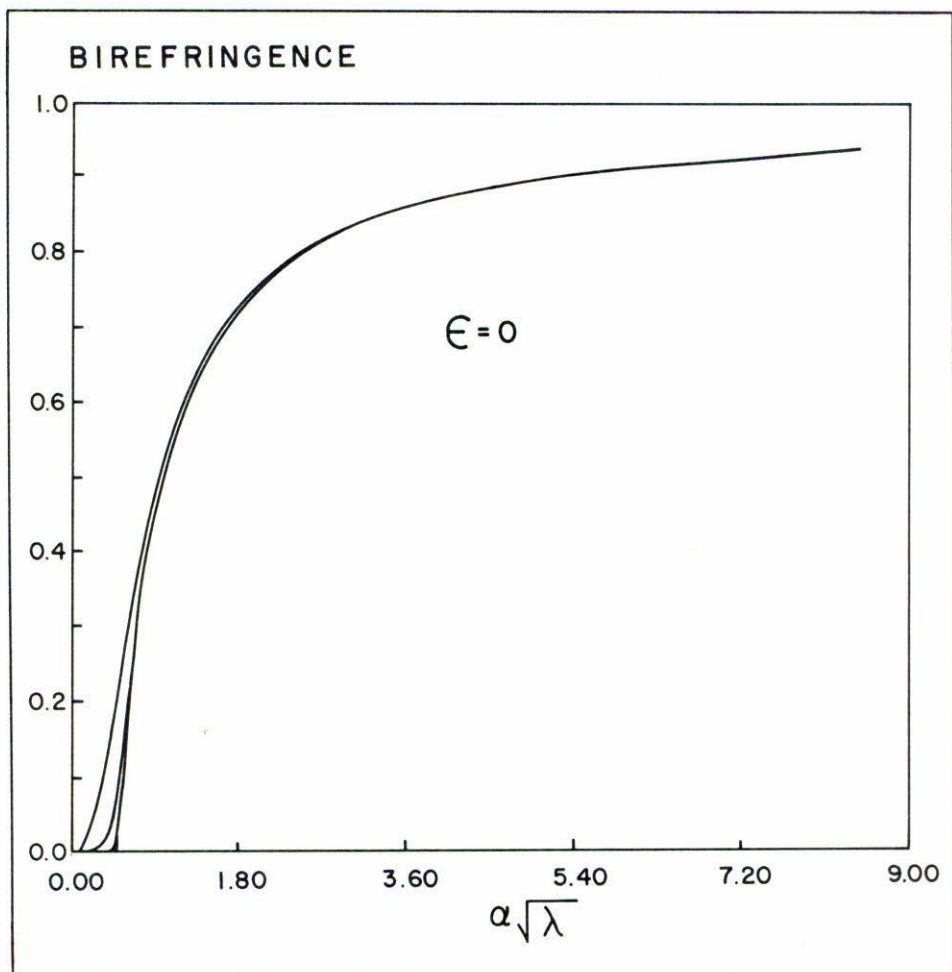
FIGURE 3. Normalized flow birefringence vs. the eigenvalue of the velocity-gradient tensor for the flow types of Fig. 2. Affine motion.

also indicates that the slip mechanism is in effect dictated by the eigenvalue of the effective velocity gradient tensor, and the quantity $\alpha\sqrt{v}$ therefore controls the degree of deformation in the system. When $\epsilon = 0$ (affine motion) the group $\alpha\sqrt{v}$ becomes $2\alpha\sqrt{\lambda}$ which
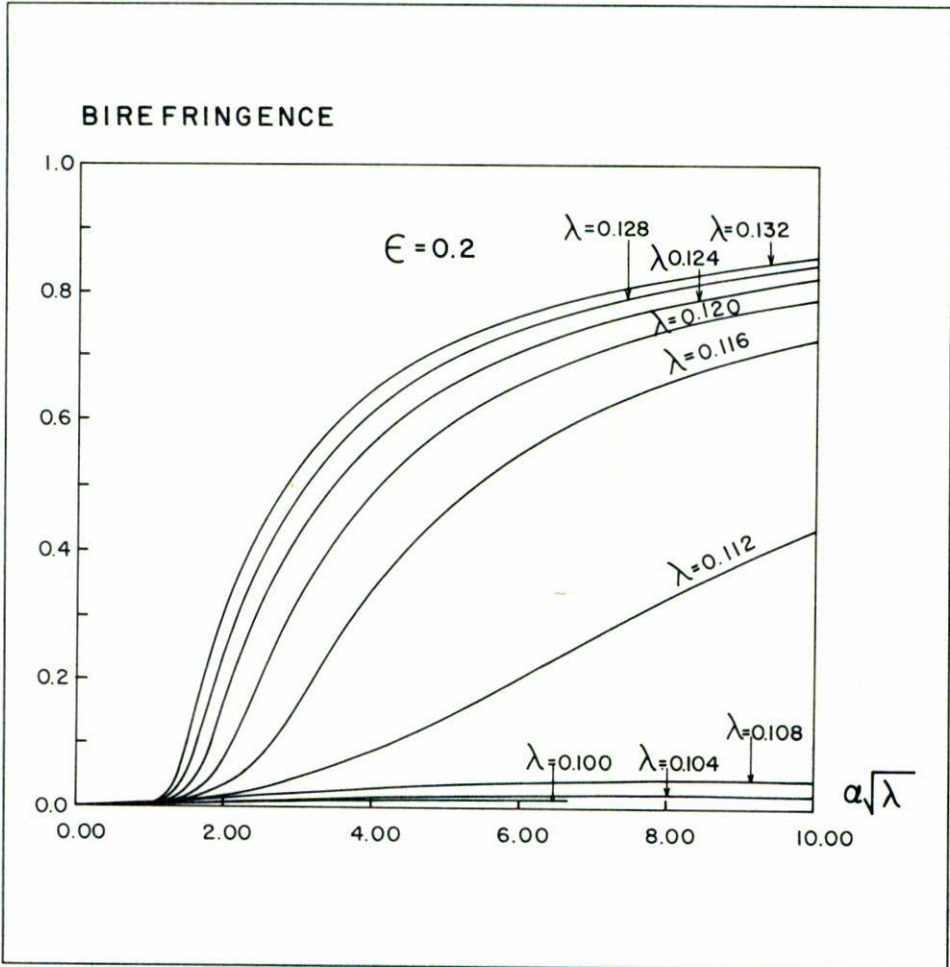
BIREFRINGENCE

FIGURE 4. Normalized flow birefringence vs. the eigenvalue of the velocity-gradient tensor for flow types in the range $0.1 \leq \lambda \leq 0.132$ with constant slip parameter ($\epsilon = 0.2$).

is exactly twice the eigenvalue of the velocity gradient tensor. For this reason, the birefringence is well correlated against $\alpha\sqrt{\lambda}$. Consequently, the correlation with $\alpha\sqrt{\lambda}$ must break down when $v = 0$,
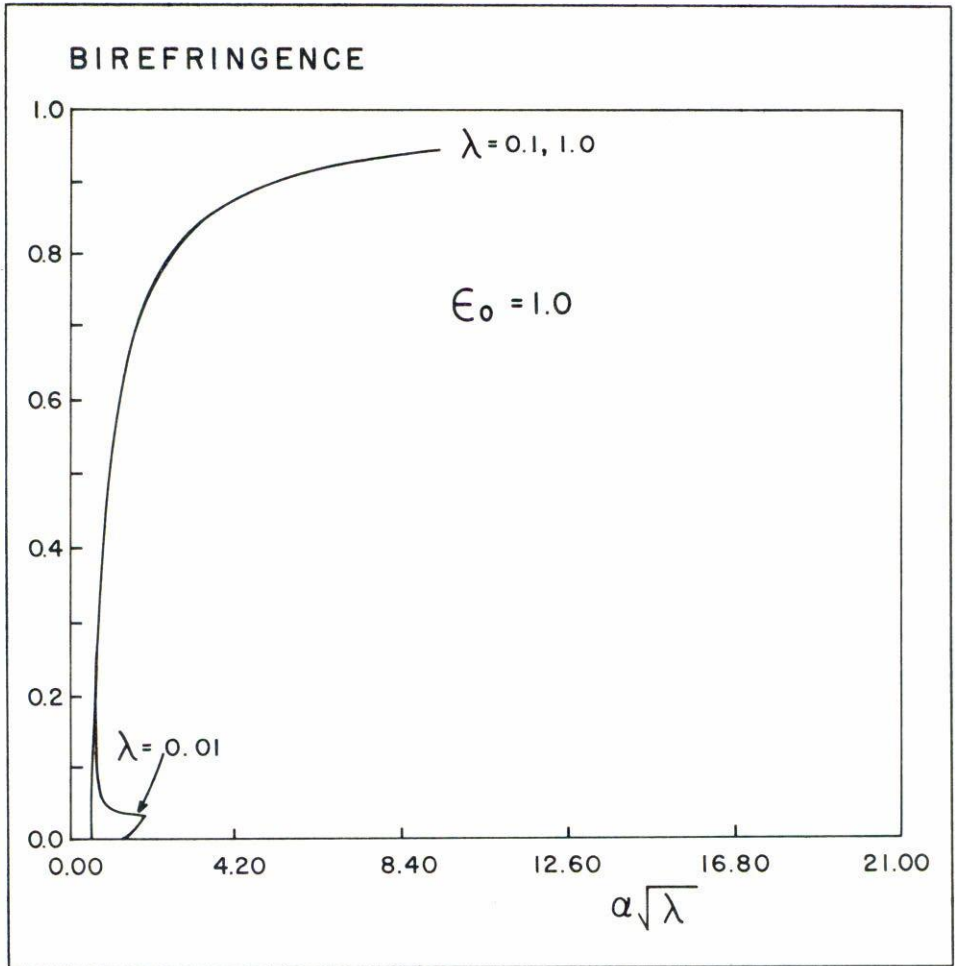
FIGURE 5. Normalized flow birefringence vs. the eigenvalue of the velocity-gradient tensor for flow types in the range $0.01 \leq \lambda \leq 1.0$ with conformation-dependent slip parameter ($\epsilon_0 = 1.0$).

which provides an estimate of the range of λ for a given value of ϵ over which the correlation will hold, when ϵ is a nonzero constant. Because of this, the relationship between ϵ and the minimum value

of λ for the correlation to hold is obtained by setting v equal to zero in Eq. (9):

$$\lambda^* = \frac{\epsilon}{2 - \epsilon}. \tag{11}$$

Fig. 4 shows results for $\epsilon = 0.2$. In this case, the correlation breaks down at $\lambda^* = 0.111$. It is observed that above this value the curves will eventually correlate. Below this value, deformation is not sufficient over the range of velocity gradients considered, so that the curves are uncorrelated.

When a conformation-dependent slip parameter is used (Eq. (4)) correlation is obtained for λ as low as 0.01 as it is depicted in Fig. 5, where the birefringence correlates with the eigenvalue of the velocity gradient tensor in the range $0.01 \leq \lambda \leq 1$. This demonstrates the importance of conformation-dependent non-affine motion in flows sufficiently close to simple shear. Also, these theoretical predictions are in qualitative agreement with experimental data to be shown in the last section. Next, the expressions for the stress tensor are worked out to the case of planar elongational flow ($\lambda = 1$).

4. Steady planar elongation

In this case, we have

$$\frac{N_1}{kT} = \frac{L}{\beta_0} \frac{4\alpha(1 - \epsilon[\langle r^2 \rangle])}{h^2 - 4\alpha^2}, \tag{12}$$

where N_1 is the elongational stress and α the elongation rate. Particularly in this case, elongated segments and a major decrease in junction concentration are produced at finite values of the slip parameter.

This result is in contrast with predictions in simple shear, where the slip mechanism produces a limited degree of deformation. (See Fig. 1, Part I).

This behaviour brings important consequences to the predictions of the macroscopic quantities. For instance, the slip mechanism is

not important in the region of high deformations. Eq. (4) shows that when $\langle r^2 \rangle \to 1, \epsilon \sim \epsilon_0$. Similarly, the stress given by

$$\tau = \frac{\beta_0}{1 - \langle r^2 \rangle} \langle \mathbf{rr} \rangle \tag{13}$$

deviates considerably from the linear spring (Hookean) behaviour at high deformations. Fig. 6 show the variation of the elongational viscosity with the elongation rate, for constant values of the slip parameter. Comparison is made with Fig. 7, where conformation dependent non-affine motion of Eq. (4) is included. It shows that same features of the case $\epsilon = 0$ in Fig. 6.

Results shown in Figs. 6 and 7 do not agree with predictions from the quadratic destruction model {1} with linear springs. In the Gaussian regime the junctions break at relatively small deformation of the segments. Therefore, it is expected that the elongational viscosity will decrease after attaining a maximum value. However, in the nonlinear regime of deformations, the network can still support higher stresses and the viscosity levels off as it is depicted in these figures. Experimental data agrees with predictions in the nonlinear regime of deformations.

5. Experimental results

Experiments suggested that birefringence measurements can be used to test the predictions for the slip mechanism or non-affine motion. The general idea is to determine the smallest value of the flow parameter λ where data correlate with the eigenvalue of the velocity gradient tensor (see Eq. (11)), and to place an upper bound on the magnitude of ϵ. In order to determine this value, it would be necessary to achieve very small values of the flow parameter, close to the region of simple-shear flow.

Frank and Mackley [2] have studied flow birefringence in flows generated by two corrotating rollers. Their experimental results show that the flow type produced between the two rollers can be placed between the two cases of simple shear flow and pure extensional
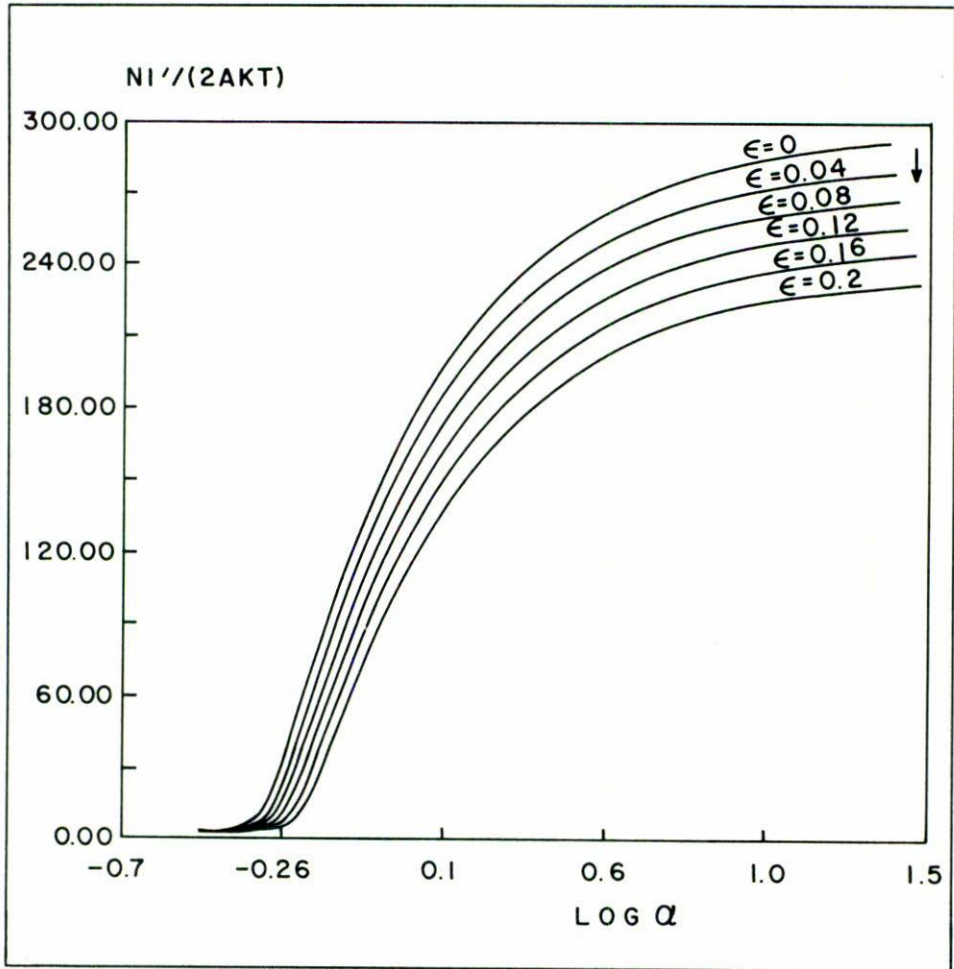
FIGURE 6. Elongational viscosity vs. elongation rate with various values of the slip parameter.

flow. The magnitude of the velocity gradient and the flow type are dependent on the separation and size of the two rollers, and they can be arranged in such a way to produce flows very near simple shear, attaining a very low value of λ $(0 < \lambda \leq 0.01)$.
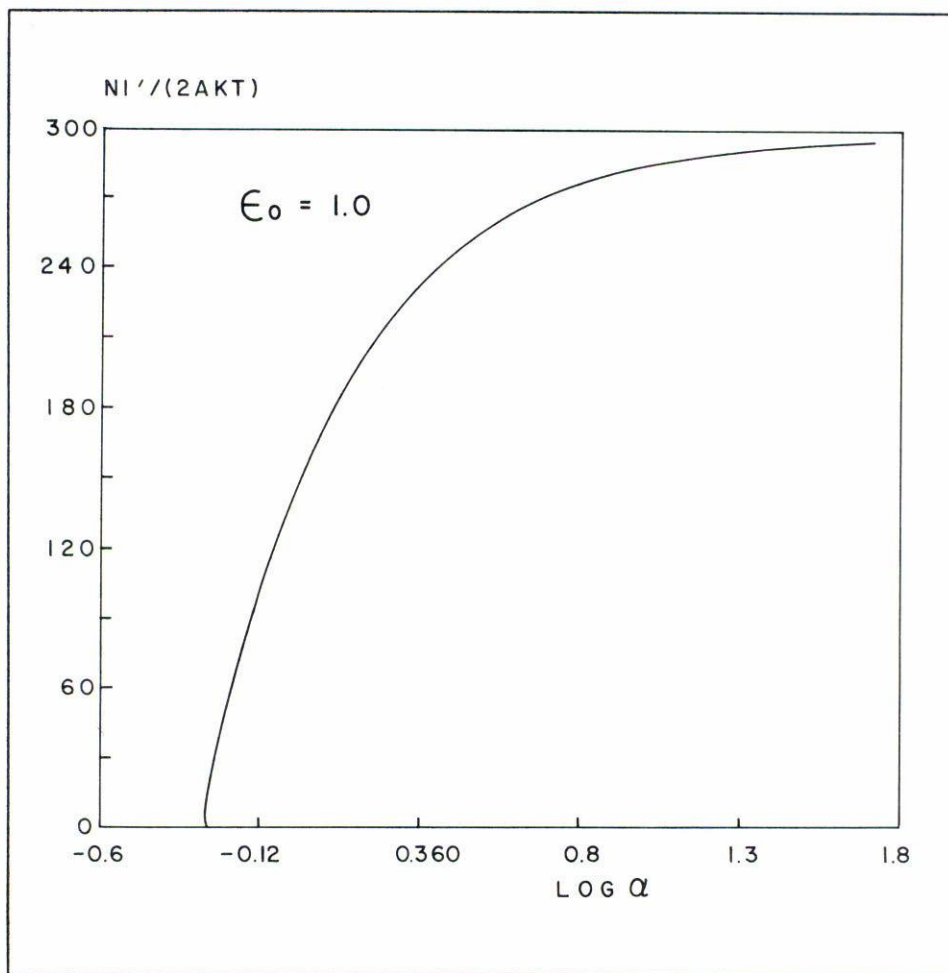
FIGURE 7. Elongational viscosity vs. elongation rate with conformation-dependent slip parameter ($\epsilon_0 = 1.0$).

Figs. 8 and 9 show the experimental birefringence plotted against eigenvalue $\alpha\sqrt{\lambda}$, for two concentrated polymeric solutions of flexible macromolecules: 1.5% Polyethylene oxide in water and 1000 PPM, 18×10^6 M.W. monodisperse Polystyrene dissolved in Tricresylphos-
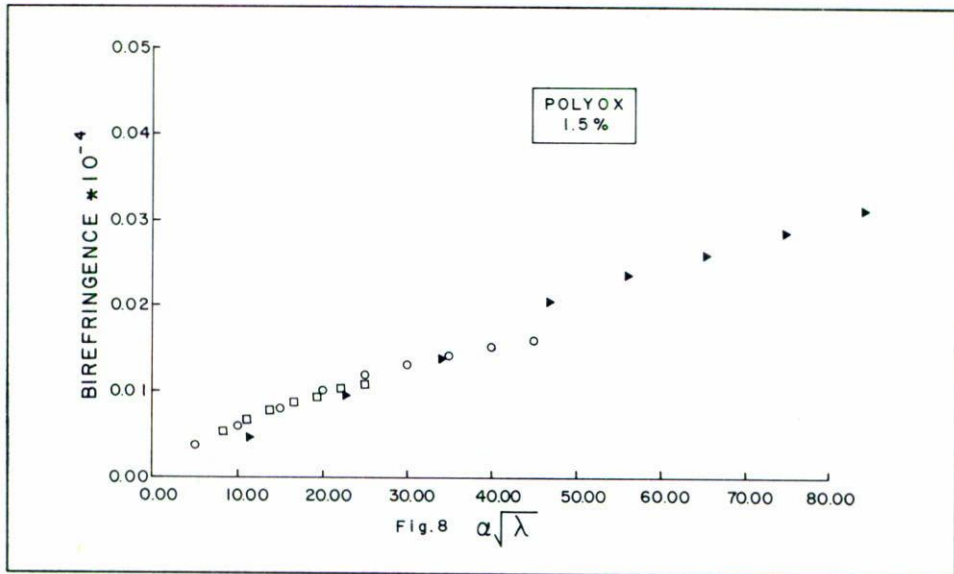
FIGURE 8. Experimental birefringence vs. the eigenvalue of the velocity-gradient tensor. 1.5% Aqueous solution of polyethylene oxide in water.
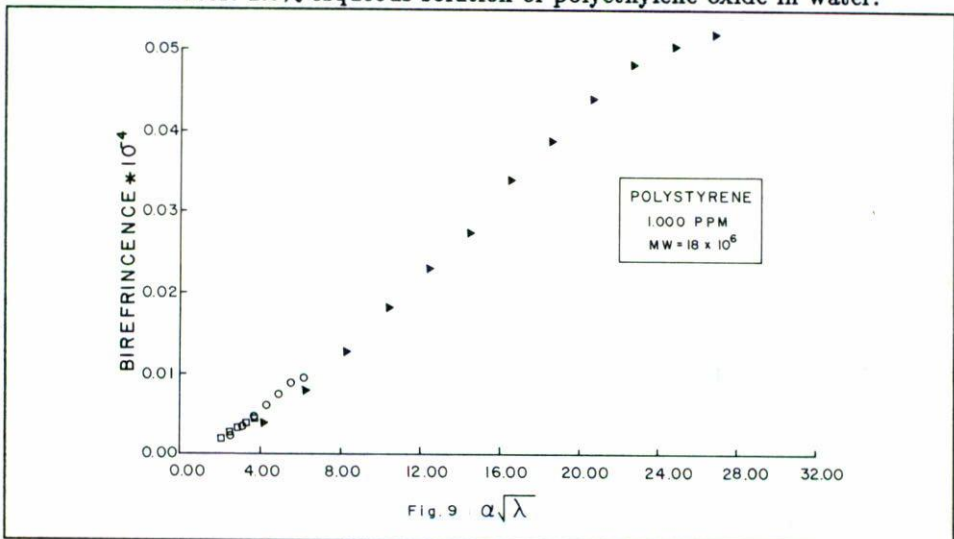

FIGURE 9. Experimental birefringence vs. the eigenvalue of the velocity-gradient tensor. 1000 PPM (18×10^6 MW) of polystyrene in tricresylphosphate.

phate. In both solutions, the flow parameter varied in the range $0.0187 \leq \lambda \leq 0.1$.

These experimental results show no bound for the magnitude of the slip parameter, since there is no breaking point for the correlation. The results can be described by taking $\epsilon = 0$ (affine motion). However, experimental results in these solutions in simple shear suggested the existence of non-affine motion. Therefore, the results are predicted qualitatively by recourse to a conformation-dependent slip parameter whose results for the birefringence also show correlation over this range of values of the flow parameter (Fig. 5).

As it has been pointed out in Part I, flows sufficiently close to simple shear cover the region of intermediate force regime. In this region, the hydrodynamic interaction tends to increase and the non-free draining character of the segments is enhanced. The underlying idea is that the structural elements of the polymer network are not stressed by the average motion of the continuum, but by a velocity field modified owing to hydrodynamic interaction. It is supposed that this effect reduces only the deformational component of the flow field, the reduction being represented by the slip parameter.

6. Conclusions

It has been already shown that extensional flow is able to deform the network segments by a large extent due to the imposed flow. Theoretical results were presented using a nonlinear expression for the destruction function which agrees with the spring force on the segments and with the assumed statistics. By considering a conformation-dependent slip parameter, it is shown that birefringence correlates with the eigenvalue of the velocity gradient tensor down to very small values of the flow parameter. This is in qualitative agreement with experiments performed in a two roll-mill apparatus on two concentrated polymeric solutions.

Acknowledgements

References

1. G.G. Fuller and L.G. Leal, *J. of Pol. Sci. Pol. Phys.* **19** (1981) 531.
2. F.C. Frank, A. Keller and H.H. Mackley, *J. Pol. Sci. Pol. Phys.* **14** (1976) 1121.